Mon. Not. R. Astron. Soc. **000**, 000–000 (0000) Printed 7 August 2015 (MN LATEX style file v2.2)

Short Gamma-Ray Bursts with Extended Emission Observed with *Swift*/BAT and *Fermi*/GBM

Y. Kaneko,[1] Z.F. Bostancı,[1,2] E. Göğüş,[1] L. Lin[1,3]
[1] *Sabancı University, Faculty of Engineering and Natural Sciences, Orhanlı-Tuzla 34956 Istanbul Turkey*
[2] *Istanbul University, Faculty of Sciences, Department of Astronomy and Space Sciences, University 34119 Istanbul, Turkey*
[3] *APC laboratory-FACe, 13 Rue Watt 75205 Paris Cedex 13 France*

ABSTRACT
Some short GRBs are followed by longer extended emission, lasting anywhere from ∼10 to ∼100 s. These short GRBs with extended emission (EE) can possess observational characteristics of both short and long GRBs (as represented by GRB 060614), and the traditional classification based on the observed duration places some of them in the long GRB class. While GRBs with EE pose a challenge to the compact binary merger scenario, they may therefore provide an important link between short and long duration events. To identify the population of GRBs with EE regardless of their initial classifications, we performed a systematic search of short GRBs with EE using all available data (up to February 2013) of both *Swift*/BAT and *Fermi*/GBM. The search identified 16 BAT and 14 GBM detected GRBs with EE, several of which are common events observed with both detectors. We investigated their spectral and temporal properties for both the spikes and the EE, and examined correlations among these parameters. Here we present the results of the systematic search as well as the properties of the identified events. Finally, their properties are also compared with short GRBs with EE observed with BATSE, identified through our previous search effort. We found several strong correlations among parameters, especially when all of the samples were combined. Based on our results, a possible progenitor scenario of two-component jet is discussed.

Key words: gamma-ray bursts: general - method:search for extended emission

1 INTRODUCTION

The progenitors of extremely energetic gamma-ray bursts (GRBs) are most likely either the core collapse of a massive star (collapsar; Woosley 1993; MacFadyen, Woosley, & Heger 2001) or the coalescence of two compact objects (neutron stars or black holes) in a binary system (see e.g., Eichler et al. 1989). An increasing number of observational facts point toward association of long GRBs (longer than a few seconds) with massive stars collapsing into black holes (Woosley & Bloom 2006) or possibly fast-rotating magnetars (Thompson, Chang & Quataert 2004). In particular, observational predictions of the collapsar scenario include association with core-collapse supernovae (SNe), and also with late-type host galaxies having active star formation.

On the other hand, for short GRBs (lasting less than a few seconds), observations so far have yielded no support, even contradictions with the collapsar scenario. There has been no SN association with any short GRBs albeit some extensive search efforts were in place (Berger 2014). Short GRBs seem to occur relatively nearby (with cosmological redshift, $z \lesssim 1$), and their host galaxies can be both early-type and late-type. Moreover, the short emission timescales and the energetics involved pose challenges for the collapsar model. Therefore, the compact-binary merger scenario remains to be the most plausible picture to account for their observational properties.

For intermediate-duration GRBs (∼5 s), however, the classification may not be clear-cut: over the last decade, a growing population of short GRBs with extended emission (EE) has emerged. These events are characterized with an initial short burst phase, followed by a much longer ($\gtrsim$ few tens of seconds) emission episode. EE components are usually (but not always) relatively dimmer and spectrally softer compared to the initial short spike. GRBs with EE exhibit several spectral and temporal properties of both short and long GRBs, therefore, could play a pivotal role in understanding the nature of both canonical burst types.

Since the first clear identification of such "hybrid" GRBs in 2006 (GRB 060614; Gehrels et al. 2006), there has been a few extensive investigations to search for more of these type of events and uncover their observational characteristics. Norris & Bonnell (2006) have identified ∼15 GRBs

with EE via visual inspection of ∼2700 bursts observed with Burst and Transient Source Experiment (BATSE) on board *Compton Gamma-Ray Observatory*, among which 8 GRBs were investigated. They found that the spectral lags for the initial spikes of these events were negligible. Bright long GRBs, on the contrary, usually display noticeable lags, with an average of ∼50−100 ms (Norris, Marani & Bonnell 2000). All of these events were classified as long GRBs with the durations, $T_{90} > 2$ s in the BATSE catalog. In addition, extended emission was also identified in a dozen short-duration GRBs observed with *Swift*/Burst Alert Telescope (BAT), in the Bayesian block representation of their lightcurves (Norris, Gehrels, & Scargle 2010, 2011; Sakamoto et al. 2011). The initial spikes of these events are also spectrally harder and displayed no spectral lags. Most of them were associated with X-ray afterglow observed with *Swift*/X-Ray Telescope (XRT), that are brighter and longer lasting than the afterglow of non-EE GRBs.

We previously searched systematically the entire BATSE GRB dataset to identify GRBs with EE that are similar to GRB 060614 (Bostancı, Kaneko & Göğüş 2013). We found 18 such GRBs with clear EE components within the BATSE data, and investigated their properties. Here, we extend our search to include all GRBs observed with *Fermi*/Gamma-ray Bust Monitor (GBM) and *Swift*/BAT before February 2013 (regardless of their T_{90} duration). A few notable advantages of extending the search to GBM and BAT events are:

(i) It increases the total sample size of GRBs with EE, providing better statistics for examining their overall properties,
(ii) About 80% of all BAT GRBs have afterglow observation with XRT, and 30% have measured redshift values; if found, the afterglow and the source-frame properties of GRBs with EE can be investigated, and
(iii) There are many GRBs observed simultaneously with GBM and BAT; if such common GRBs are associated with EE, more in-depth information about the EE could be obtained, as well as shed light on systematic differences between the instruments.

In this paper, we present the results of our systematic search for short GRBs with EE using the data of *Swift*/BAT and *Fermi*/GBM, and subsequent analysis of the events identified with the search. Below, the event selection and the search methodology are described in §2, and the search results and investigation of the detection sensitivity are presented in §3. Then in §4, we present the properties of the candidate events based on our analysis. Finally, we discuss the implication of our results in §5.

2 EVENT SELECTION AND SEARCH METHODOLOGY

We first selected all events that consist of initial short spikes, and the selected events were then subjected to the EE search described in detail below. We used all available data up to January 31, 2013 for both BAT and GBM. We applied essentially identical search methodology to both BAT data and GBM data, which was also used for our previous systematic search with BATSE data (Bostancı, Kaneko & Göğüş 2013). However, the data coverage, reduction procedures, and the data types are different for the two instruments, and therefore, slight adjustments were made according to the detector characteristics, which we describe in this section.

2.1 Data and Event Selection

For both BAT and GBM events, the first sample selection was made based on the burst duration (T_{90}) published in their catalogs (Paciesas et al. 2012; Sakamoto et al. 2011). We note that T_{90} is calculated in slightly different energy bands for the two detectors; 15−350 keV for BAT and 50−300 keV for GBM, due to the difference in the sensitivities and energy coverage of the detectors. All short GRBs with $T_{90} \leqslant 5$ s were included in the systematic search for EE. Additionally, to identify and include in the search all GRBs with correct morphology (i.e., containing initial short spikes regardless of their T_{90}), we first subjected all of the long GRBs to a morphological test as described next.

BAT: There are 685 GRBs detected with BAT between 20 November 2004 and 31 January 2013, among which 95 are short ($T_{90} \leqslant 5$ s) and 590 are long GRBs ($T_{90} > 5$ s).

For all of the long events, we extracted background-subtracted (i.e., mask-weighted) lightcurves in 15−350 keV with 64-ms time resolution, using `batbinevt` included in HEASOFT version 6.12. The count rates were then multiplied by the number of enabled detectors for each event to obtain the total count rates.

GBM: There are 1040 GRBs detected with GBM between 1 August 2008 and 31 January 2013, among which 246 are short ($T_{90} \leqslant 5$ s) 794 are long GRBs ($T_{90} > 5$ s).

For each of the long GRBs, we used Time-Tagged Event (TTE) burst data binned to 64-ms time resolution, and subtracted the background rate, which is an average count rate of a pre-burst interval (∼ T_0−30 s to T_0−2 s, where T_0 is the burst trigger time).

For both BAT and GBM, we then subjected the lightcurves of the long GRBs to the following morphological criteria:

(i) The burst peak occurs before T_0+5 s, and
(ii) The count rates remain below 30% (or 40% for some BAT events with low peak rate of <11k count/s) of the peak count rate for at least 50% of the rest of the duration after the peak time until T_0+5 s.

We found 33 BAT (103 GBM) events out of 590 (808) long GRBs that matched the morphological criteria. We then searched for EE in these events together with the 95 (184) short GRBs. The total numbers of events subjected to the search was 128 for BAT and 287 for GBM.

2.2 Background Determination

Correct background modeling is crucial in detecting the EE components, as EE can be weak and only slightly above the background. For BAT, the background is not an issue since the lightcurve produced is mask-weighted, meaning that the lightcurve is essentially background free if there is no other bright source (usually known) in the field of view.

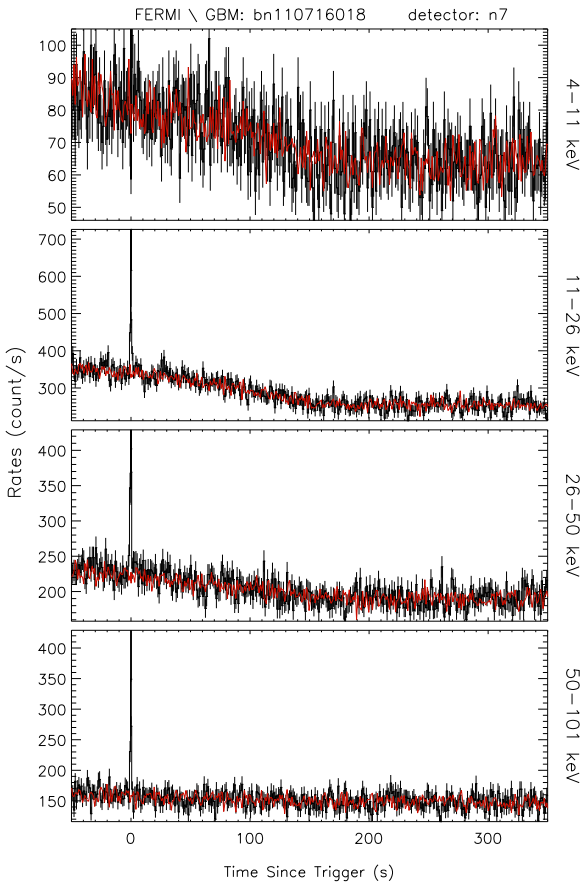

Figure 1. An example GBM lightcurve in four energy bands (indicated on the right side of each panel), showing the orbital background (red).

For GBM, on the other hand, the background rates at the time of a transient event have to be estimated by modeling, based on its long-term behavior in all energy band. The GBM background can be quite variable over a relatively-long period of time, which could hinder a simple polynomial interpolation. Therefore, as suggested by Fitzpatrick et al. (2011) and as used also for our previous EE search with the BATSE data, we determined background rates for GBM events from the data of adjacent days. The *Fermi* satellite was at the same coordinates every ∼15 orbits (corresponding to ∼24 hours), and the spacecraft rocking angle was the same every 2 orbits. Thus, we used either the average of $T_0 \pm 30$ orbits or the average of $T_0 \pm 14$ and $T_0 \pm 16$ orbits (see also Fitzpatrick et al. 2011). When both types of orbital data were available, we compared the average rms of the count rates over a pre-burst interval of T_0-50 to T_0-10 s of the triggered and the orbital data, and the orbital background that better matched the data rms was used for the search. An example of such orbital background lightcurve is shown in Figure 1.

Using the orbital background, we generated the background-subtracted lightcurves for 257 GRBs out of the 287 GBM GRBs. There were 30 GRBs for which the data of the previous orbits were either not available or incomplete, and the orbital background could not be used. Visual inspection of these events revealed two bursts that clearly showed extended emission, so we used low-order polynomial interpolation to model the background rates for the two events, which are indicated accordingly in Table 1. The other 28 bursts were excluded from the sample. Additionally, for one event also showing EE (GRB 121029), the orbital background was available but clearly not matching; therefore, the background was modeled with a polynomial function around the burst time also for this event.

2.3 EE Search Criteria and Method

Our EE search is based on Signal-to-Noise Ratio (SNR) of binned lightcurve. The EE search criteria we employed here were identical to those used in our previous search with BATSE data. The criteria were defined based on previously-observed short GRBs with EE, such as GRB 060614 (Gehrels et al. 2006) and those found by Norris & Bonnell (2006), all of which seem to constitute the hybrid class of short and long GRBs. We first extracted energy-resolved lightcurves for all of the GRBs in our sample, as follows:

BAT: We extracted 1-s resolution lightcurves both background-subtracted and with background (i.e., unweighted), for each of the 128 GRBs in four energy bands; 15−25, 25−50, 50−100, and 100−150 keV. We used the unweighted lightcurves for determining the background fluctuation (σ values).

GBM: For each of the 260 GRBs, we subtracted background for two detectors in which the event appeared brightest, using daily CTIME data rebinned to 1-s resolution. The CTIME data provide 8 energy channels in ∼5−2000 keV.

For both BAT and GBM, we subsequently binned the lightcurves with 4-s resolution between T_0+5 and T_0+350 s and calculated the SNR of each bin. We used the lightcurves of two energy bands: <50 keV and 50−100 keV. The lowest energy thresholds were 15 for BAT, and ∼10 keV for GBM. The search algorithm positively identified EE when SNR $\geqslant 1.5\sigma$ above background for at least consecutive 12 s (3 bins) in any of these energy bands. In case of GBM, the criteria had to be met in both detectors for the positive identification of the EE, as GBM data did not provide specific directional information. We further checked the lightcurves of all 12 NaI detectors of GBM candidates so as to exclude the possibility that the detected EE was due to another soft transient source.

3 SEARCH RESULTS AND DETECTION SENSITIVITIES

Using these criteria, we found 37 BAT GRBs and 72 GBM GRBs as candidates for short GRBs with EE. We subsequently inspected each one of these candidates, and manually eliminated ones with obvious background issues (e.g., Earth occultation of another source or data mismatch over longer period), as well as those that are clearly multi-episodic long GRBs based on the morphology and the spectral hardness. We additionally excluded the events whose EE

was not visible at all in any other energy range, to reduce the possibility of chance detection.

After the manual filtering, we were left with 16 BAT GRBs and 14 GBM GRBs as the true EE candidates. We list all of the identified events in Table 1 with their T_{90}, durations of the spikes and the EE (see §3.1), and afterglow observation information where available. The lightcurves of all of these candidate events are available online,[1] one of which is shown as an example in Figure 2. As seen in Table 1, most of the BAT events with EE have associated afterglow observations in x-ray and optical bands, and 8 events have their redshift values available. There are 3 events for which X-ray flares are seen in their X-ray lightcurves observed with *Swift* X-Ray Telescope (XRT). One event's flare actually coincides with the EE detected here (GRB 100212A; see §4.2 for the discussion). The redshift values are mostly $\lesssim$1, which is consistent with short GRBs' redshift distribution (Berger 2014). One exception to this is GRB070506 with $z = 2.31$. This is an exceptionally high z value for a short GRB.

Among these, 5 GRBs were common events observed both with BAT and with GBM, which we also indicate in Table 1 with C1 or C2. For two of the five common events, EE was only detected in BAT in our search. The common events were additionally subjected to joint spectral analysis and discussed separately in §4.3. Our search also detected EE components in the GBM data of two additional common events, GRB 090518 and GRB 091127, extending up to ∼300 s and ∼15 s after the trigger, respectively. However, we found out that GRB 090518 EE was an activity from Vela X-1 coinciding with the GRB direction (C. Wilson-Hodge, private communication), which was flagged by the fact that the BAT lightcurve showed no indication of the EE. GRB 091127 was a long GRB associated with SN 2009nz (Cobb et al. 2010). Thus these events were excluded from the list of candidates.

We note that although these 30 candidate GRBs presented in Table 1 all cleared the search criteria, some of them may be of different nature based solely on their lightcurves. They all contain initial short spikes of $\lesssim$5 s indeed; however, there are cases where, for example, there is a preceding weaker peak that makes the actual duration of the spike longer (GRB 090131), or the entire burst is pretty spiky that the subsequent "extended emission" appears to be rather a continued episode of a long GRB (GRB 091120). Nonetheless, as it is difficult to classify events only from their lightcurves, we did not exclude these events from the list. In addition, for one of the BAT events (GRB 051016B), Vela X-1 with varying flux was in the BAT field-of-view at the time of the burst trigger. Therefore, we caution that the possibility of contribution of this X-ray source to the EE detected in GRB 051016B cannot be ruled out. All of these candidate events were subjected to the subsequent analysis.

Finally, the candidates also include 7 of the 12 BAT GRBs with EE previously identified by Norris, Gehrels, & Scargle (2010) and Sakamoto et al. (2011). The other 5 were not found in our search because the extended emission components of 4 of them were too short and too weak for our search criteria, and one of them had a spike >5 s so did not meet our morphological criteria. We note that albeit short and weak, there are visible indications of extended emission in the lightcurves of these 5 events.

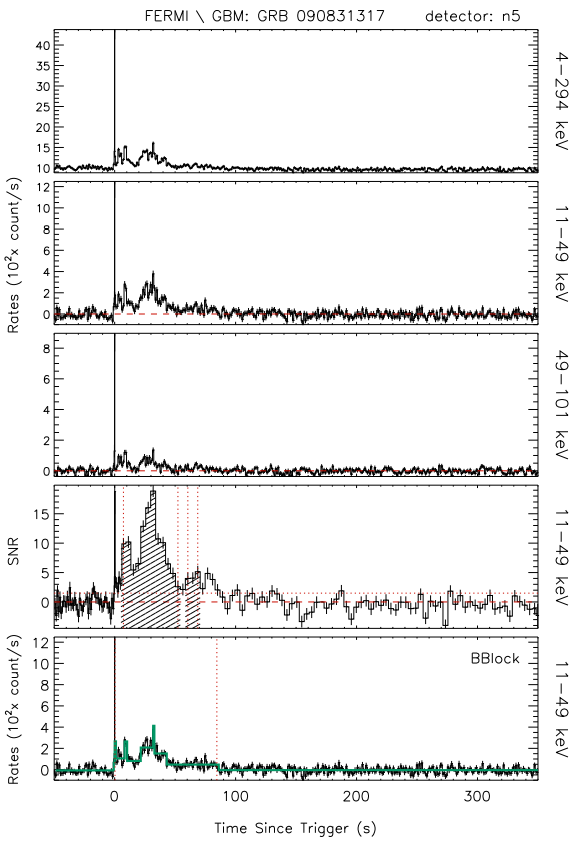

Figure 2. An example GBM lightcurve in three energy bands as indicated on the right side of each panel. The bottom two panels are the binned SNR history and the Bayesian block lightcurve (green histogram), in which the EE selection is indicated in red vertical dashed lines. Further figures can be viewed in the electronic version of the article.[1]

3.1 Durations of Spikes and EE

It is noteworthy that none of our 30 candidate events can be classified as "short GRBs" by the conventional definition of $T_{90} < 2$ s. However, they all consist of short spikes, so we systematically determined the durations of the spike and the EE separately for each event with Bayesian block (BB) method (Scargle et al. 2013). The BB representation simplifies the lightcurve with a series of step function that could easily reveal local structures in the time series. The duration, then, was the beginning and the end of the spike or EE blocks. We adopted the algorithm of Scargle et al. (2013) to generate a BB lightcurve for each event in the energy range in which the EE was detected (usually < 50 keV). We used the mask-tagged data for BAT and background-subtracted CTIME data for GBM, with 64-ms and 1-s resolutions for this purpose.

We first applied the BB method using the 1-s resolution data on the interval, 50 s before and 400 s after the

[1] Available at
http://people.sabanciuniv.edu/yuki/GRBEE_BAT_GBM_all.pdf

Table 1. Properties of the candidates for GRBs with EE identified in the search. The duration of the spike and the EE were determined using Bayesian block method. C1 and C2 indicate the common events observed with both BAT and GBM. C1 events' EE were only identified in either BAT or GBM data whereas C2 events' EE were identified in both datasets.

	GRB name	T_0 Time UT	T_{90}[a] (s)	$T_{\rm spike}$ (s)	$T_{\rm EE}$ (s)	$B_{\rm spike}$[b] (s)	$B_{\rm EE}$[b] (s)	Afterglow[c]	z	X-ray flare
	BAT									
	050724[d]	12:34:09	96	2.76	107	−0.02	3.04	XOR	0.258	T_0+$10^4 s$
	051016B	18:28:09	4	4.03	33	0.07	4.23	XO	0.9364	T_0+409s
	060614[d]	12:43:49	108.7	5.89	169	-1.55	7.24	XO	0.125	–
	061006[d]	16:45:51	129.9	2.05	113	-23.2	2	XO	0.4377	–
	061210[d]	12:20:39	85.3	0.13	77	0.21	1.04	X	0.4095	–
	070506	5:35:58	4.3	5.25	15	3.75	38	XO	2.31	–
	070714B[d]	4:59:29	64	2.88	39	−0.8	32.29	XO	0.92	–
	080503[d]	12:26:13	170	0.38	147	0.11	6	XO	–	–
C1	090531B[d]	18:35:56	80	1.02	54	0.29	2.04	X?	–	–
	090927	10:07:16	2.2	2.18	28	0.06	2.95	XO	1.37	–
C1	100212A[e]	14:07:22	136	2.18	135	−0.32	1.86	XO	–	T_0+∼100s
C2	100522A	3:45:52	35.3	3.97	15	−0.68	23.86	X	–	–
C2	110207A	11:17:20	80.3	3.07	137	0.184	10.6	–	–	–
C2	110402A	0:12:57	60.9	2.52	82	3.56	6.08	XO	–	–
	111121A	16:26:24	119	2.37	61	0.04	4	X	–	–
	121014A	20:11:56	80	0.96	81	−0.10	14.8	–	–	–
	GBM									
	080807[f]	23:50:33	19.07	1.28	27	−0.12	1.15	–	–	–
	090131	2:09:21	35.07	7.81	23	1.98	22.27	–	–	–
	090820	12:13:17	15.3	0.77	7	-0.19	8.32	–	–	–
	090831	07:36:37	39.42	0.45	86	−0.12	0.32	–	–	–
	091120	4:34:40	50.18	2.82	52	0.00	2.81	–	–	–
	100517	3:42:08	30.46	1.41	11	−0.12	22.02	–	–	–
C2	100522	3:45:52	35.33	3.97	13	−0.64	26.49	X	–	–
C2	110207	11:17:20	37.89	3.07[g]	38	−0.32	2.68	–	–	–
C2	110402	0:12:58	35.65	1.41[g]	39	−0.32	1.08	XO	–	–
	110824	0:13:10	76.61	1.54	93	0.00	1.54	–	–	–
	111228	10:52:50	2.94	6.53	30	−0.51	25.7	–	–	–
	120402	16:04:01	20.22	5.63	19	−2.30	4.16	–	–	–
	120605[f]	10:52:16	18.11	2.82	8	−0.57	12.41	–	–	–
	121029[f]	8:24:20	15.81	0.38	6	−0.12	10.75	–	–	–

[a] Taken from Sakamoto et al. (2011) and Paciesas et al. (2012)
[b] The begining of the spike and the EE since trigger time
[c] X = X-ray, O = optical, R = radio
The afterglow and redshift information was obtained from J. Greiner's web page at http://www.mpe.mpg.de/j̃cg/grbgen.html as well as from the XRT lightcurve repository at http://www.swift.ac.uk/xrt_curves
[d] Also identified as GRBs with EE in Norris, Gehrels, & Scargle (2010) using Bayesian block method
[e] Double-episodic event; see §4.2 for more information
[f] Background rates were modelled with low-order polynomial interpolation
[g] Calculated using 1.024 resolution

burst trigger time for each burst to determine $T_{\rm EE}$. For the peak duration, we utilized the 64-ms data for both BAT and GBM, for the interval 40 s prior and 20 s after the burst trigger time. We could not measure peak duration of two GBM events (GRBs 110207 and 110402) due to insufficient statistic. Therefore, we listed peak durations of these two in 1-s domain in Table 1. In cases where the end of the spike and the beginning of the EE were not clear-cut, we took the beginning of the block with the lowest intensity around T_0+5 s as the beginning of $T_{\rm EE}$. In the lightcurves available from the links given above, the BB lightcurve of each event is also shown with the intervals of spike and EE indicated. An example is shown in Figure 2.

The resulting BB duration of the spikes and EE are presented in Table 1 as $T_{\rm spike}$ and $T_{\rm EE}$ respectively, along with the start time of the spike and the EE ($B_{\rm spike}$ and $B_{\rm EE}$). In Figure 3, we compare the durations of the spikes and the EE components of our candidate events to the T_{90} distributions of all BAT and GBM GRBs observed up to January 31, 2013. The majority of our candidate events have spikes that are longer than the 2-s division line, up to ∼10 s. We caution, however, that the population comparison in Figure 3 is associated with a caveat: the GBM and BAT durations are T_{90} values (i.e., time during which 90% of photons are emitted) determined in the most sensitive energy range of each instrument, in photon space for GBM (Paciesas et al. 2012) and mostly with the BB method for BAT (Sakamoto et al. 2011). Here, our duration is the total emission time in the energy range in which the EE was detected. We further note that, the duration values of the 3 common GRBs with EE identi-

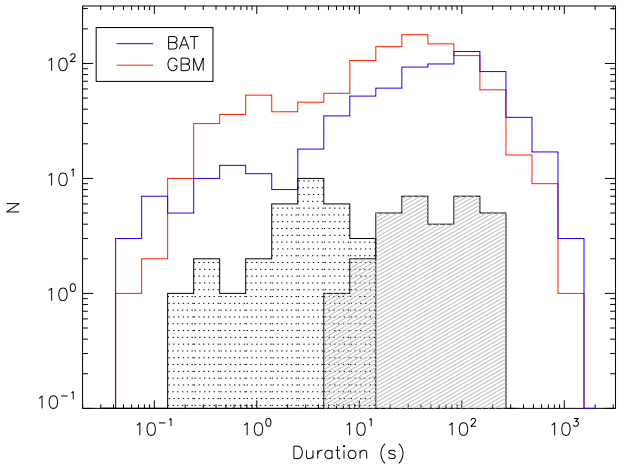

Figure 3. Distribution of the duration of the spikes (dotted) and EE (hashed) of all 30 candidates, shown against the T_{90} distribution of all GRBs observed up to January 31, 2013 (BAT in blue and GBM in red).

fied in both BAT and GBM data (GRBs 100522A, 110207A, and 110402A), are not necessarily consistent between the BAT data and GBM data. This is because the EE components may have been identified in different energy ranges, in addition to the difference between the sensitivities of the two instruments. So in the histogram, they are included with their BAT duration and GBM duration independently.

3.2 Detection Rates and Sensitivities

To probe the sensitivity limits of both BAT and GBM and the rate of the false-positive EE detection, we have simulated large sets of EE lightcurves (LCs) and subjected them to our EE search algorithm, which we describe in details below.

For each event and for each instrument, we first simulated the EE using the actual Bayesian block representation of the EE LC (in the energy band where the EE was identified), and added random noise to the simulated EE. The noise distribution used here is Gaussian for BAT data and Poisson for GBM data, decided based on the real error distributions. We then added the simulated, noise-added EE to the "burst-free" background LC of the same energy range, which are:

BAT: mask-weighted LC of the time interval from T_0+150 to 900 s, displaced by −150 s (so the background LC starts at T_0) for most of the bursts. In the cases of bursts with long EE or data with shorter time coverage, the time interval was from $T_0 + (1.2 \times T_{\rm EE,end})$ to MAX(data time).

GBM: real data for pre-/post- time intervals which is the start time of the data to T_0−10 s and $T_{\rm EE,end}$+10 s to the end time of the data. In between, we use the background model fitted to the pre-/post-burst time intervals using a 2nd order polynomial function.

We show an example of simulated EE LCs and their background in Figure 4 for GRB 100522A (a common event observed with both GBM and BAT). As seen in the figure,

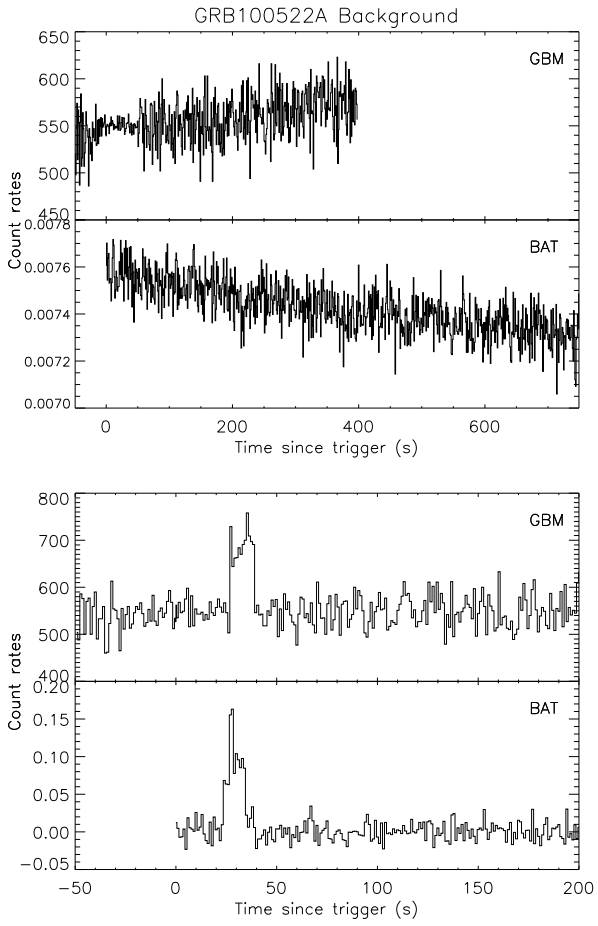

Figure 4. [*Top*] Background lightcurve used in the simulations for GRB 100522A, a common event observed with both GBM and BAT. Here, we show the orbital background for GBM and the burst-free lightcurve of the time interval after the actual detected EE, as described in §3.2. [*Bottom*] Simulated lightcurve for the same event, including noise-added EE. The EE components shown here were simulated based on their Bayesian block time profile and amplitude, in the energy range of actual EE identification.

the simulated EE was placed at the actual start time of the EE determined by the Bayesian method (= $B_{\rm EE}$) for each instrument.

3.2.1 EE detection sensitivity

For each event and instrument, we varied the amplitude of the simulated EE component nominally with 2×, 1×, 0.9−0.1× (in 0.1 steps), and 0× the actual Bayesian block amplitudes. This was done for 3 energy bands: 15−25, 25−50, and 15−50 keV, one of which was used for the original Bayesian block LC for each event. We simulated 10,000 LCs for each amplitude and energy band, and subjected them to our EE search algorithm. For each set of LCs, our aim was to determine the amplitude level at which at least 90% of the simulated LCs could be detected. To better constrain the 90 percentile amplitude level, we re-

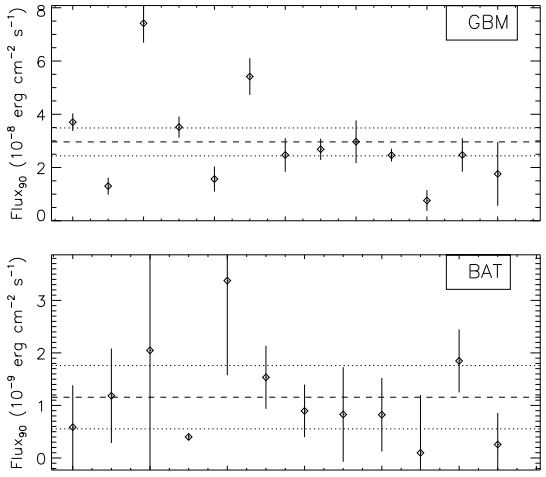

Figure 5. The energy flux level for the 14 GBM events [*top*] and 16 BAT events [*bottom*] above which more than 90% of the simulated EE were detected. The x-axis is the event numbers. The average flux level of $2.9(3) \times 10^{-8}$ ergs cm^{-2} s^{-1}(GBM) and $1.2(6) \times 10^{-9}$ ergs cm^{-2} s^{-1} (BAT) is indicated by the dashed line, with 1s standard deviation (dotted lines).

peated the same procedure in narrower amplitude interval, with finer amplitude steps as necessary. We find that the 90 percentile amplitudes of both BAT and GBM samples are anti-correlated with their corresponding flux, as expected.

Finally, in order to determine the detection sensitivities while minimizing the effect of various LC morphology on the detection rates, we also simulated all EE with single step functions of the actual EE durations and 10-σ amplitudes. Again, we simulated 10,000 LCs for the same set of amplitude values and energy bands as above, and subjected them to our EE search algorithm. Based on our simulation results, we determined the 90 percentile EE detection flux level (i.e., 90 percentile amplitude times the average EE flux) for each event. We then determined the average 90 percentile flux for each instrument. We find that the average energy flux level above which more than 90% of the simulated EE are detected is $2.9(3) \times 10^{-8}$ ergs cm^{-2} s^{-1} (for GBM) and $1.2(6) \times 10^{-9}$ ergs cm^{-2} s^{-1} (for BAT) in 15−50 keV (see Figure 5).

3.2.2 False detection rates of our search method

As stated at the beginning of this section, the search actually yielded more potential EE candidates than what we present in this paper. We went through the 5-panel lightcurves (e.g., Figure 2) one by one for these potential candidates, and excluded the ones with obvious background issues, obvious long GRBs, or the ones with EE seen only in single energy band. Then, our final list of candidates included 16 BAT GRBs and 14 GBM GRBs. From these numbers, we could say that the inferred false detection rates of our search, with the specific set of criteria for the specific types of EE, are 57% and 79%. Although these numbers may seem high, we believe that the fact that we went through all the potential candidate lightcurves and filtered out the actual falsely-detected events, makes this not an issue for a concern.

Lastly, as an alternative way to probe the false detection rate due to the data fluctuations and/or the choice of our background models, we also searched for 12-s 1.5σ deficit in the SNR LCs for all events that were subjected to the original EE search. The search identified such deficits in 6 BAT and 4 GBM events. Among the 6 BAT deficits 4 of them are only seen in 50-100 keV band and well isolated from the bursts by >150 s. The other 2 deficits were detected only in 25-50 keV band. One of them starts at 230 s after the burst; however, the other one (for GRB 121017A) was detected at ∼20 s after the burst, which may have been identified as an EE candidate if this had been an excess, and the indication of the deficit is also seen in 15–25 keV. Thus, the false detection rate based on the deficit search is 1/128 (<1%) for the BAT sample. The deficit found for the 4 GBM events were all clearly due to mismatched orbital background data. Therefore, for our GBM sample, the false detection rate based on the deficit search is even lower than that of the BAT sample.

4 PROPERTIES OF THE EE EVENTS

4.1 Spectral Lags

One of the main characteristics that makes some GRBs with EE "short" GRBs is that the initial spikes usually show no (or close to nil) spectral lags. Thus, we calculated the spectral lags for the initial spikes of all of these events, as well as for the EE components where possible. We used lightcurves with various time resolutions of 8 to 512 ms (for both BAT and GBM) in the energy bands of 50–100 keV and 15–25 keV for BAT, and 100–300 keV and 25–50 keV for GBM, unless otherwise noted. The time interval used for each event was the spike or EE duration presented in Table 1. For each event, we determined a cross-correlation function between the lightcurves of the two energy bands, which was subsequently fitted with a cubic function. The peak of the fitted cubic function was taken as the lag. The uncertainties in the lags were estimated with the same simulation method that we used previously for the BATSE sample, which is described in Bostancı, Kaneko & Göğüş (2013).

The spectral lag values that we found are presented in Table 2. For 20 events (9 BAT and 11 GBM), in which the EE was bright enough to allow lag calculations, the lag values for the EE are also shown in the table. Although some of the errors are large, the average lags are 19 ms for the spikes and 122 ms for the extended emission. In Figure 6, we show spectral lags as a function of their duration ($T_{\rm spike}$ or $T_{\rm EE}$). For a comparison, we also over-plot the values found from our previous analysis of BATSE EE GRBs. There is an indication of a positive correlation between the spectral lags and the duration ($T_{\rm spike}$ or $T_{\rm EE}$) within the BAT sample as well as when all samples are combined (BAT + GBM + BATSE; see §4.4, albeit large uncertainties associated with some values. We also looked at the correlations with z-corrected (source frame) durations for the 8 events with known redshift values but found null results.

4.2 Spectral Analysis

In order to examine spectral properties of these short GRBs with EE as well as to obtain their energetics, we performed

Table 2. Spectral lags calculated in 50–100 keV/15–25 keV for BAT and 100–300 keV/25–50 keV for GBM events unless otherwise noted

GRB name	Spike Lags (ms)	Spike Err (ms)	EE Lags (ms)	EE Err (ms)
BAT				
050724	6.29	5.28	–	–
051016B	4.58	3.32	–	–
060614	5.83	5.61	5.46	5.39
061006	17.92	16.32	96.93	96.70
061210	6.05	4.80	–	–
070506	39.23	29.30	494.43	296.48*
070714B	8.03	7.78	–	–
080503	–7.56	4.82	40.51	8.95*
090531B	5.21	4.07	–	–
090927	4.77	2.38**	–	–
100212A	2.53	2.42	255.14	204.83
100522A	26.36	25.77	78.48	64.86
110207A	3.15	2.78	38.33	37.34
110402A	32.93	28.64	40.39	37.43
111121A	1.00	0.93	–	–
121014A	–17.30	13.59	596.32	560.79
GBM				
080807	–3.38	3.54	46.18	44.18
090131	101.84	95.49	89.10	79.18
090820	–0.01	0.49**	196.86	131.38**
090831	28.97	19.88	23.72	28.57
091120	57.50	51.34	41.98	42.35
100517	76.22	62.79	-82.24	76.50
100522	35.14	32.29	–	–
110207	22.29	18.27	62.39	66.86
110402	5.80	5.50	89.05	48.67
110824	29.54	24.06	59.04	55.70
111228	27.40	24.13	–	–
120402	2.52	0.64	–	–
120605	43.27	38.69	203.24	127.11**
121029	12.00	8.52	70.89	63.26

* lag calculated in 25–50 keV/15–25 keV
** lag calculated in 50–100 keV/25–50 keV

spectral analysis of these events using RMFIT[2] version 4.0rc1. For each event, we analyzed the spectra of the spike and the EE separately. The time intervals of the spike and EE spectra were matched to those given in Table 1.

For the BAT events, we extracted spectra with an energy range of 15−150 keV (80 energy channels) and generated corresponding detector response matrices using `batdrmgen`, which utilizes the online calibration database. For the GBM events, we used TTE data providing 128 energy channels in ∼5–2000 keV binned to 64-ms time resolution. The actual fitted energy range was ∼8–1000 keV after excluding several low-energy channels and the high-energy overflow channel (Gruber et al. 2014). For each event, we selected a set of NaI detectors with detector-to-source angles less than 60^o (Paciesas et al. 2012), and fit the data of these detectors simultaneously. Since some of the EE components were rather dim, the accurate background modeling was essential for the spectral analysis also. We modeled the background spectrum of each of the GBM event with a polynomial function, and subsequently compared it to match the orbital background we used in the search procedure. To account for a possible systematic normalization offset between the multiple detectors, we also included multiplicative "effective area correction" factor (EAC) in the initial fits using spike spectra of the bursts. We did find, however, in each case, the normalization factors were very close to 1 in most cases and were fixed in the final fits.

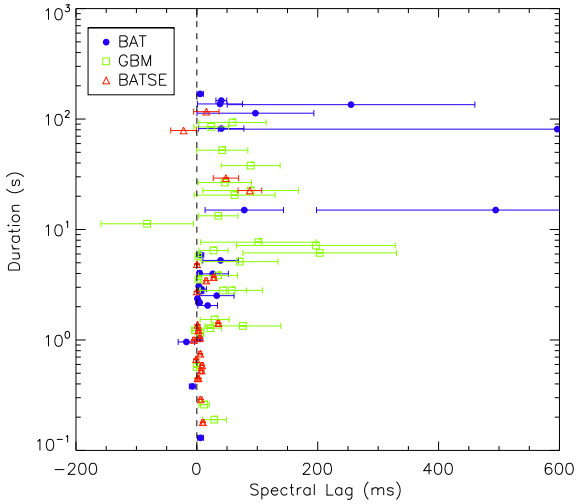

Figure 6. Spectral lag vs. duration ($T_{\rm spike}$ and $T_{\rm EE}$) of the 30 candidate events. BAT and GBM events are shown with different symbols and colors. For comparison, the values for BATSE GRBs with EE from our previous work are also included.

We fitted each spectrum (spike and EE separately) with three models: a power law (PWRL), cut-off power law (or "Comptonized"; COMP), and the Band function (BAND; Band et al. 1993), by minimizing χ^2. The best-fit model for each spectrum was subsequently determined based on the improvements in their χ^2 values for additional degrees of freedom. In Table 3, we present the best-fit model parameters along with the energy fluence, peak flux, and hardness ratios. The hardness ratio here was calculated in photon space using the best-fit spectral parameters. Both the spikes and the EE of all of the BAT events were sufficiently described with PWRL, as expected for the narrow-band spectra of BAT. On the other hand, some GBM spectra are described better with COMP model.

Interestingly, we noticed that the BAT lightcurve of GRB 100212A displayed a secondary spike (at T+80 s, see Figure 7) dimmer than the initial spike at T_0, followed by secondary EE. This second episode (both spike and the EE) is actually seen as a X-ray flare in *Swift* XRT data of the same event[3] . We attempted to extract the spectra of the secondary spike and the EE that follows using BAT data (as well as BAT+GBM), but the component was too weak for a spectral analysis. Nevertheless, it is obvious from these lightcurves that the second episode is much softer than the

[2] R. S. Mallozzi, R. D. Preece, & M. S. Briggs, "RMFIT, A Lightcurve and Spectral Analysis Tool," © Robert D. Preece, University of Alabama in Huntsville.

[3] The XRT lightcurve is available at http://www.swift.ac.uk/xrt_curves/00412081/

Table 3. Summary of spectral fit results of GRBs with EE.

GRB Name	Component	Model	λ	$E_{\rm peak}$ (keV)	χ^2/dof	Energy[b] Fluence	$F_{\rm peak}$[c]	Hardness Ratio[d]
BAT								
050724	Spike	PWRL	−1.67 ± 0.12		62.5 / 56	4.3 ± 0.2	6.8 ± 0.7	1.25 ± 0.14
	EE	PWRL	−2.04 ± 0.18		71.7 / 56	7.3 ± 0.9	0.3 ± 0.3	0.98 ± 0.17
051016B	Spike	PWRL	−2.42 ± 0.17		72.8 / 56	1.8 ± 0.2	1.1 ± 0.3	0.75 ± 0.14
	EE	PWRL	−2.87 ± 0.57		47.1 / 56	1.2 ± 0.3	0.3 ± 0.2	0.55 ± 0.38
060614	Spike	PWRL	−1.67 ± 0.04		46.6 / 56	40.4 ± 1.1	15.5 ± 1.7	1.26 ± 0.05
	EE	PWRL	−2.10 ± 0.02		55.0 / 56	115.3 ± 1.2	4.0 ± 1.0	0.93 ± 0.02
061006	Spike	PWRL	−1.07 ± 0.06		38.0 / 56	7.4 ± 0.3	12.3 ± 0.8	1.89 ± 0.09
	EE	PWRL	−2.23 ± 0.16		54.5 / 56	8.6 ± 0.8	0.5 ± 0.3	0.85 ± 0.14
061210	Spike	PWRL	−0.75 ± 0.14		34.9 / 56	4.2 ± 0.4	24.9 ± 1.7	2.39 ± 0.31
	EE*	PWRL	−1.73 ± 0.20		85.0 / 56	9.2 ± 1.2	—	1.21 ± 0.23
070506	Spike	PWRL	−1.79 ± 0.12		52.4 / 56	2.6 ± 0.2	0.5 ± 0.2	1.14 ± 0.15
	EE	PWRL	−2.88 ± 0.71		40.4 / 56	0.6 ± 0.2	0.4 ± 0.3	0.53 ± 0.45
070714B	Spike	PWRL	−1.10 ± 0.07		51.7 / 56	6.8 ± 0.3	5.7 ± 0.6	1.87 ± 0.11
	EE	PWRL	−2.33 ± 0.34		40.5 / 56	1.8 ± 0.4	0.3 ± 0.2	0.80 ± 0.30
080503	Spike	PWRL	−1.85 ± 0.39		61.9 / 56	0.6 ± 0.2	1.8 ± 0.4	1.07 ± 0.40
	EE	PWRL	−1.93 ± 0.08		44.2 / 56	19.4 ± 0.9	0.1 ± 0.1	1.06 ± 0.08
090531B	Spike	PWRL	−1.25 ± 0.12		58.4 / 56	2.4 ± 0.2	2.1 ± 0.4	1.68 ± 0.17
	EE	PWRL	−1.79 ± 0.17		54.1 / 56	5.0 ± 0.1	0.5 ± 0.3	1.16 ± 0.19
090927	Spike	PWRL	−1.88 ± 0.16		54.9 / 56	2.2 ± 0.3	2.1 ± 0.5	1.09 ± 0.18
	EE	PWRL	−1.98 ± 0.45		67.5 / 56	1.9 ± 0.6	0.8 ± 0.4	1.00 ± 0.46
100212A	Spike	PWRL	−1.42 ± 0.10		53.3 / 56	3.1 ± 0.2	2.0 ± 0.4	1.50 ± 0.13
	EE	PWRL	−2.47 ± 0.21		64.3 / 56	6.1 ± 0.8	0.6 ± 0.3	0.73 ± 0.24
100522A	Spike	PWRL	−1.67 ± 0.04		45.5 / 56	17.0 ± 0.5	6.9 ± 0.7	1.26 ± 0.05
	EE	PWRL	−2.56 ± 0.10		45.3 / 56	6.1 ± 0.3	0.6 ± 0.3	0.68 ± 0.07
110207A	Spike	PWRL	−1.29 ± 0.14		46.6 / 56	2.5 ± 0.3	6.6 ± 0.8	1.63 ± 0.21
	EE	PWRL	−1.46 ± 0.09		48.2 / 56	17.0 ± 1.1	1.3 ± 0.4	1.45 ± 0.12
110402A	Spike	PWRL	−1.04 ± 0.15		55.7 / 56	9.9 ± 0.9	10.5 ± 2.1	1.94 ± 0.27
	EE	PWRL	−1.93 ± 0.14		52.7 / 56	29.7 ± 2.7	2.7 ± 1.1	1.05 ± 0.14
111121A	Spike	PWRL	−1.22 ± 0.06		67.2 / 56	10.9 ± 0.4	16.0 ± 1.3	1.72 ± 0.09
	EE	PWRL	−2.02 ± 0.10		58.6 / 56	11.8 ± 0.7	0.6 ± 0.3	1.02 ± 0.10
121014A	Spike	PWRL	−2.27 ± 0.16		60.8 / 56	1.5 ± 0.2	2.1 ± 0.4	0.83 ± 0.15
	EE	PWRL	−2.00 ± 0.14		51.4 / 56	9.7 ± 0.8	1.2 ± 0.3	1.00 ± 0.13
GBM								
080807	Spike	PWRL	−1.08 ± 0.02		487.7 / 480	11.1 ± 0.3	23.0 ± 2.3	3.72 ± 0.16
	EE	PWRL	−1.33 ± 0.04		523.9 / 480	18.5 ± 0.9	9.5 ± 1.8	2.91 ± 0.18
090131	Spike	COMP	−1.16 ± 0.04	56.7 ± 1.2	743.9 / 476	30.5 ± 0.4	40.6 ± 3.0	0.77 ± 0.04
	EE	COMP	−1.49 ± 0.03	154.5± 14.0	642.7 / 476	49.6 ± 0.7	48.8 ± 3.8	1.74 ± 0.05
090820	Spike	PWRL	−1.68 ± 0.04		377.4 / 356	4.3 ± 0.2	9.0 ± 1.7	2.11 ± 0.16
	EE	PWRL	−2.22 ± 0.06		409.5 / 356	7.2 ± 0.5	9.7 ± 1.8	1.30 ± 0.20
090831	Spike	PWRL	−1.34 ± 0.03		258.1 / 235	7.1 ± 0.3	51.6 ± 3.3	2.91 ± 0.16
	EE	COMP	−1.65 ± 0.06	532 ± 422	218.5 / 234	112.2 ± 3.4	24.0 ± 3.6	2.03 ± 0.12
091120	Spike	COMP	−0.76 ± 0.05	277.7± 18.7	515.3 / 470	35.1 ± 0.5	28.5 ± 3.7	2.93 ± 0.08
	EE	COMP	−1.10 ± 0.03	114.4± 3.9	631.8 / 470	192.3 ± 2.5	37.9 ± 4.2	1.52 ± 0.04
100517	Spike	COMP	−0.69 ± 0.14	92.7 ± 6.8	328.2 / 354	9.2 ± 0.4	22.7 ± 3.2	0.05 ± 0.02
	EE	COMP	−1.39 ± 0.19	26.8 ± 3.2	367.2 / 354	14.0 ± 0.8	6.5 ± 1.5	0.36 ± 0.12
100522	Spike	COMP	−0.91 ± 0.07	143.8±10.2	445.7 / 470	24.7 ± 0.6	18.9 ± 2.7	1.83 ± 0.09
	EE	PWRL	−2.21 ± 0.07		466.3 / 471	9.9 ± 0.8	4.7 ± 1.5	1.32 ± 0.23
110207	Spike	PWRL	−1.25 ± 0.05		363.1 / 351	5.1 ± 0.3	14.2 ± 2.0	3.54 ± 0.38
	EE	PWRL	−1.23 ± 0.06		353.1 / 351	22.3 ± 1.5	10.3 ± 1.9	3.24 ± 0.33
110402	Spike	PWRL	−1.18 ± 0.09		232.5 / 235	4.2 ± 0.5	34.3 ± 3.5	3.38 ± 0.59
	EE	PWRL	−1.43 ± 0.05		265.6 / 235	58.5 ± 3.1	9.3 ± 2.4	2.68 ± 0.22
110824	Spike	PWRL	−1.02 ± 0.02		493.4 / 475	23.3 ± 0.4	41.2 ± 2.8	3.92 ± 0.12
	EE	PWRL	−1.59 ± 0.03		541.2 / 475	69.4 ± 2.2	25.7 ± 2.4	2.30 ± 0.12
111228	Spike	COMP	−0.99 ± 0.08	33.9 ± 0.9	476.8 / 475	25.7 ± 0.5	18.9 ± 2.4	0.30 ± 0.04
	EE**	-	—		—	—	—	—-
120402	Spike	COMP	−1.16 ± 0.08	50.2 ± 2.2	236.8 / 235	22.8 ± 0.7	15.2 ± 2.3	0.66 ± 0.08
	EE	PWRL	−2.12 ± 0.13		293.8 / 235	4.7 ± 0.8	5.2 ± 1.7	1.35 ± 0.45
120605	Spike	COMP	−1.13 ± 0.07	375.7±80.1	403.9 / 351	16.7 ± 0.5	28.4 ± 3.7	2.70 ± 0.14
	EE	PWRL	−1.98 ± 0.06		338.7 / 352	6.6 ± 0.5	6.4 ± 1.6	1.62 ± 0.23
121029	Spike	COMP	−0.74 ± 0.15	338.3±68.7	545.7 / 561	4.4 ± 0.2	19.7 ± 2.8	3.25 ± 0.26
	EE	COMP	−0.34 ± 0.06	178.6± 6.1	577.7 / 561	52.6 ± 0.7	40.4 ± 4.3	2.48 ± 0.06

All uncertainties are 1σ.

[a] in units of 10^{-5} photon cm^{-2} s^{-2} keV^{-1}

[b] in units of 10^{-7} erg cm^{-2} and calculated in the 15−350 keV range

[c] in units of 10^{-7} erg cm^{-2} s^{-1} and calculated in the 15−350 keV range with 64-ms resolution

[d] calculated in the 25−50 keV and 50−100 keV ranges for BAT and the 50−100 keV and 100−300 keV ranges for GBM

* no enough statistic for $F_{\rm peak}$ calculation.

** could not perform the spectral fit due to its weak nature

first spike and the first EE (at $\sim T$+10 s). For the spectral analysis of EE of this event presented in Table 3, the duration used as the EE includes the first EE and the entire second episode.

4.3 Common Events

There were a total of 5 GRBs with EE that were observed with both BAT and GBM. For 3 of them EE was identified in both BAT and GBM data in our search (see Table 4 for a summary). The BAT and GBM lightcurves of two example common events are shown in Figure 7.

The EE of these two events were identified only in BAT data. Generally speaking, non-detection of EE by GBM may naturally be expected for some weak, soft EE, since BAT has larger effective area over the lower energy range of 10–100 keV than GBM NaI detectors (Stamatikos 2009).

For these 5 common events, we performed joint spectral analysis using both BAT and GBM data of the spikes and the EE. The time intervals of the joint analysis were chosen considering the start and end times of each component of both BAT and GBM data. Then, the earlier start time and later end time of the two were taken as the joint analysis time interval. The exact time intervals are limited by the resolution of GBM data; In order to match the time intervals of both spectra analyzed jointly, we extracted BAT spectra of all these common events with the selected time intervals of the GBM spectra. Moreover, we initially included the EAC factors in the joint fits to account for possible systematic discrepancy between the BAT and GBM NaI data; however, the factors were always close to unity and therefore, not needed in the final fits.

In Figure 8, we compare the spectral indices found in the joint analysis with those found in the single-detector analysis (BAT-only and GBM-only). Most of the joint spectra of both spikes and EE were still best described by PWRL, and there was one case (100522A) in which COMP was better fit to the spectra. In that case, the low-energy power-law index (α) values are shown in the Figure and indicated as such. Although the BAT energy range used for the spectral analysis (15−150 keV) lies well within the GBM energy range (8−1000 keV), the joint analysis constrained the parameters better in almost all cases as seen in the Figure. The parameters found in the joint analysis of the spikes and EE are more consistent with those found in the GBM-only and BAT-only analysis respectively, although the GBM and BAT parameters are usually consistent within 1–2σ (if the same models are used). The joint analysis illustrates that using only the BAT spectrum is not always sufficient to determine the real spectral shape due to the its narrow coverage in relatively softer energy range; nonetheless, adding the BAT data to broader GBM spectra can help better constrain the spectral parameters.

4.4 Correlations

To study the general properties of the spikes and the EE of the 30 candidate events, we looked for correlations among their spectral parameters, durations, lags, and flux/fluence. The correlations were searched separately for the BAT and GBM samples to reduce the chance of finding a false correlation caused by possible systematic differences between

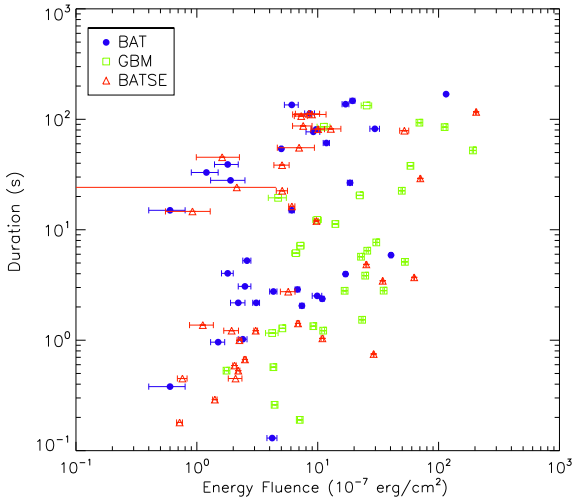

Figure 9. Energy fluence vs. duration for all of the events. A correlation was found in all datasets individually. A correlation with increased significance ($P \sim 10^{-6}$) were found when all datasets were combined.

the samples. Moreover, we studied the correlations in several different sampling: within the spikes of the 30 events, within the EE components, as well as spike vs. EE, and the spikes and EE all together.

The exact parameters used for the correlation study are: burst's duration (T_{90}), durations of each component ($T_{\rm spike}$ and $T_{\rm EE}$), spectral lag, best-fit spectral parameters, energy fluence, peak energy flux, hardness ratio, and total burst energy fluence. For the 8 events with z measurements, we also looked at their isotropic-equivalent total energy ($E_{\rm iso}$), luminosity, and source-frame durations (i.e., $T/(1+z)$). We also compared the parameters we found in this study to the BATSE sample from our previous study (Bostancı, Kaneko & Göğüş 2013).

We list in Table 5 only the pairs of parameters between which a significant correlation (with a chance probability, $P \lesssim 10^{-4}$) was found in at least one of the datasets of BAT, GBM, or BATSE. Only the correlation between the duration and energy fluence is 'universal', found to be significant in all three data sets (see Table 5 and Figure 9). However, including this one, the significance of many correlations greatly improved when all datasets are combined. The most significant combined correlations are found between peak flux and spectral index ($P \sim 10^{-14}$), duration and hardness ratio ($P \sim 10^{-10}$), and peak flux and hardness ratio ($P \sim 10^{-9}$). The correlations between peak flux of spike and EE ($P \sim 10^{-6}$) also became significant only when all data were combined (see Figure 10). It is possible that such an improvement is artificially introduced by putting together samples, each of which has some degree of systematic biases in observed parameters. Uncertainties in cross calibrations among these three instruments may also be a contributing factor. Nonetheless, the most significant combined correlations such as the ones mentioned above (also shown in Figure 10) may indicate that the correlations exist when including wider ranges of the parameters, and that each of these instruments is detecting different population in these parameter space. These correlations simply became

Table 4. List of common events observed with both BAT and GBM.

GRB name	EE detected in the search in BAT	in GBM
090531B	yes	no but visible in LC
100212A	yes	no
100522A	yes	yes
110207A	yes	yes
110402A	yes	yes

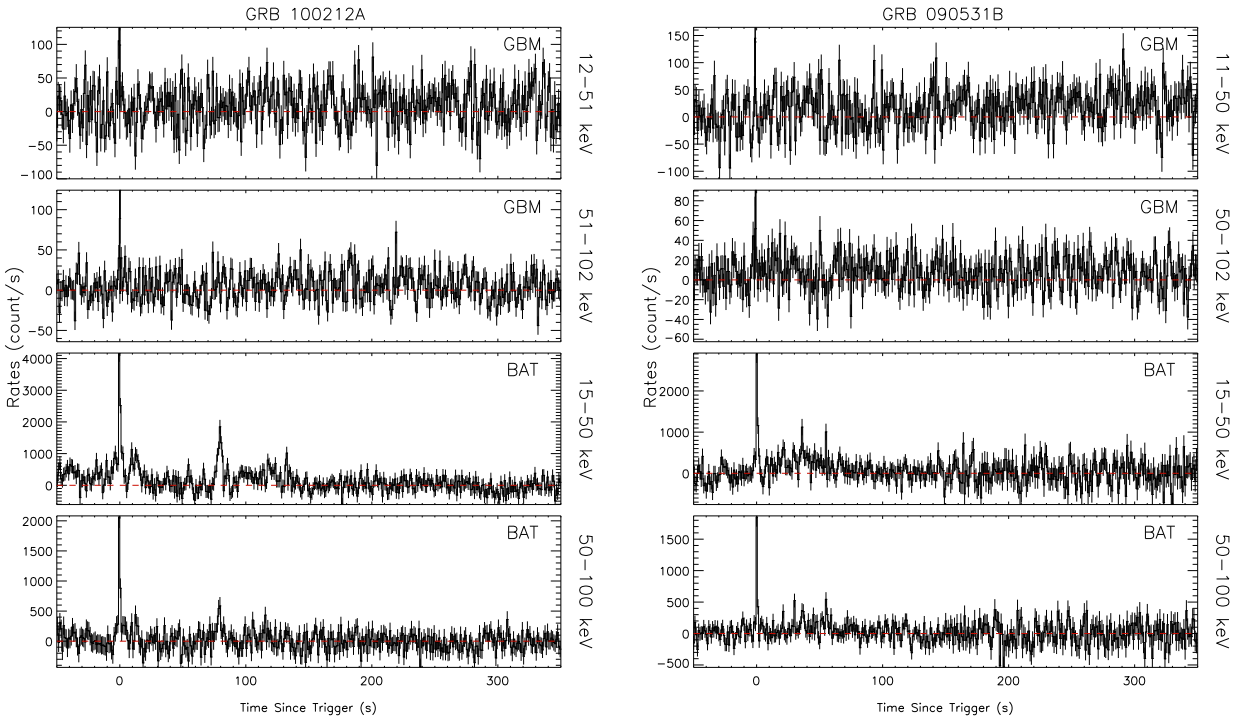

Figure 7. The background-subtracted lightcurves of GRBs 100212A and 090531B observed both with BAT (bottom two panels) and with GBM (top two panels). The EE was identified only in the BAT data.

Table 5. List of parameter pairs that are significantly correlated in at least one of the event samples of BAT, GBM, or BATSE. ALL means BAT+GBM+BATSE all combined. Spearman's rank-order correlation coefficient, ρ with a chance probability, P, are shown. N is the number of data points. The boldface indicates where significant correlations ($P < 10^{-4}$) were found.

Parameters		BAT			GBM			BATSE			ALL		
		ρ	P	N	ρ	P	N	ρ	P	N	ρ	P	N
Duration	Spectral Lag#	**0.68**	**1.4E−4**	26	0.46	2.0E−2	25	0.18	4.2E−1	22	**0.54**	**9.4E−7**	73
Duration	Peak Flux	**−0.56**	**9.5E−4**	32	−0.27	1.5E−1	29	**−0.63**	**5.2E−5**	35	**−0.52**	**5.8E−8**	96
Peak Flux	Hardness Ratio*	**0.70**	**7.3E−6**	32	0.45	1.4E−2	29	0.44	8.3E−3	35	**0.55**	**5.6E−9**	96
Duration	Hardness Ratio*	−0.46	7.6E−3	32	−0.44	1.8E−2	29	**−0.56**	**4.6E−4**	35	**−0.59**	**1.6E−10**	96
Duration	Energy Fluence	0.48	6.0E−3	32	**0.65**	**1.4E−4**	29	**0.54**	**7.4E−4**	35	**0.46**	**3.1E−6**	96
Peak Flux	PWRL Index	**0.71**	**6.3E−6**	32	0.53	2.8E−3	29	**0.60**	**1.4E−4**	35	**0.68**	**1.5E−14**	96
Peak Flux, Spike	Peak Flux, EE	0.17	5.3E−1	16	0.53	5.1E−2	14	0.3	2.4E−1	17	**0.61**	**4.3E−6**	47
Hardness Ratio*, Spike	Hardness Ratio*, EE	0.36	1.8E−1	16	**0.82**	**2.9E−4**	14	−0.01	9.7E−1	17	0.27	6.4E−2	47

Some spectral lag values are associated with large uncertainties, which are not taken into account here (see Table 2)
* The hardness ratio are calculated in 50−100/25−50 keV for BAT, 100−300/50−100 keV for GBM and BATSE events. For the combined correlation (i.e., ALL), all ratio are calculated in 50−100/25−50 keV.

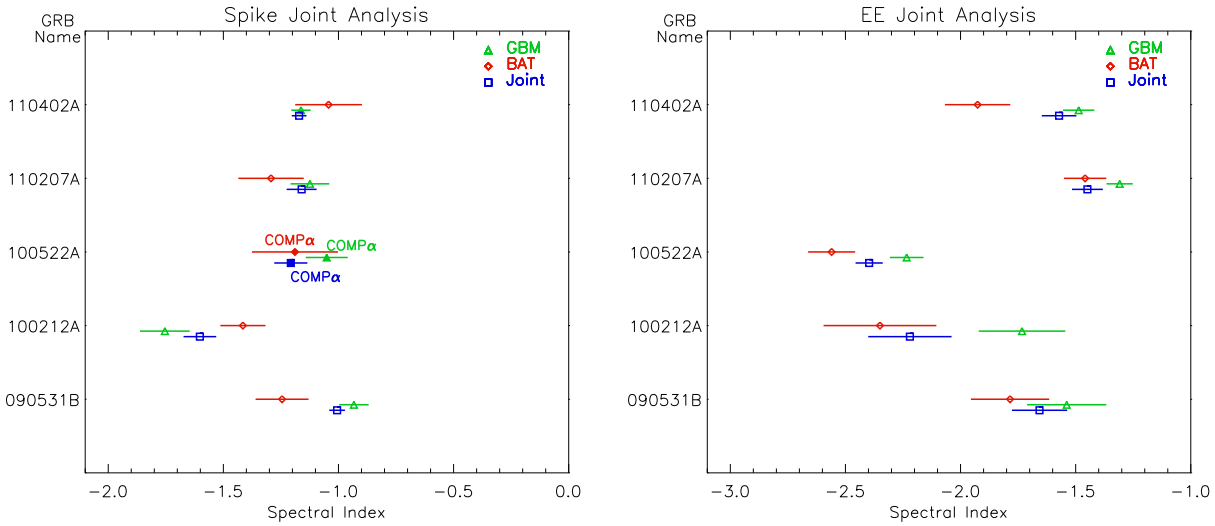

Figure 8. The best-fit PWRL indices of the spikes (left) and EE (right) of the 5 common events observed with both BAT and GBM. In the cases where COMP provides better fits, the low-energy indices (α) are also shown. The indices found in single detector analysis (either BAT or GBM) and in joint analysis (BAT+GBM) are shown for each event.

statistically much more significant with more data points. As we showed in the simulations in §3.2, the EE detection sensitivities of BAT and GBM differs by an order of magnitude, which may explain the scatter in the peak flux values of among the three samples.

For the 8 events for which there are redshift measurements, we also looked at source-frame parameters, such as redshift-corrected durations, energy fluence, isotropic-equivalent total energy, and luminosity. All of these 8 events are best described with PWRL. The sample size is small but we did not find any correlations using the source-frame parameters. It is known that the peak luminosity and the spectral lag are anti-correlated only for long GRBs (Norris, Marani & Bonnell 2000; Ukwatta et al. 2010). We compare our sample's peak luminosity and lags to the long-GRB correlation in Figure 11. There are 3 events among the 8 for which we were able to calculate spectral lag of the EE, so those are also included in the plots. These data points are circled. All of them, including the EE, lie away from the correlation found for long GRBs but are consistent with GRB 060614 as well as other short GRBs. A few of the EE with longer lags are similar in values to sub-luminous long GRBs, sometimes associated with supernovae; e.g., GRB 031203.

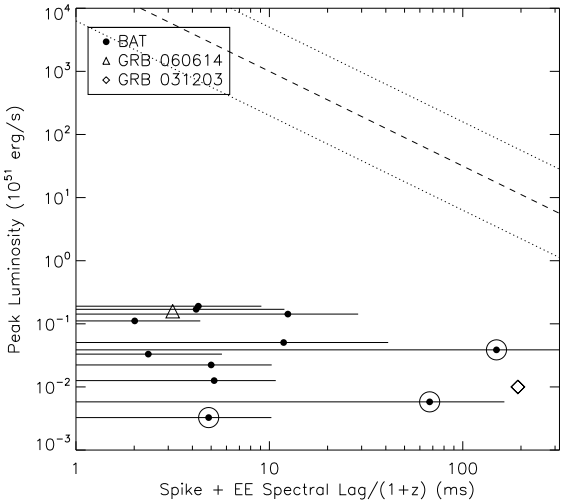

Figure 11. Peak luminosity vs. spectral lag for the 8 events with redshift values. EE values available for 3 events are circled. The dashed line shows the correlation for long GRBs (a power law of index -1.5) with 1σ confidence level shown as dotted lines (Ukwatta et al. 2010). The values of GRB 060614 is also shown as a reference (triangle).

4.5 Spike vs. EE properties

It has been reported in literature as well as in our previous study of the BATSE GRBs with EE that the EE components tend to be spectrally softer than the initial spikes. Therefore, the spectral indices of longer EE components are expected to be smaller than those of the shorter spikes. The PWRL indices of the spikes and EE (for all BAT, GBM, and BATSE samples) are compared in Figure 12, in which we see a clear indication of EE indices being softer, although no significant correlations were found in any of the three samples. We also compare in Figure 12 the hardness ratio of spike versus EE. We also see the indication of the spikes being spectrally harder than the corresponding EE, but only within the GBM sample was a significant positive correlation found (Spearman's rank-order correlation coefficient, $\rho = 0.82$ with a chance probability, $P \sim 10^{-4}$, see Table 5).

Furthermore, as stated earlier, the hardness ratio is negatively correlated with duration, especially when all datasets are combined ($\rho = -0.59, P \sim 10^{-10}$, see also Figure 10). This reinforces the statement that the spikes are harder than the EE, but additionally, this demonstrates that the anti-correlation also exists within the spikes or EE components.

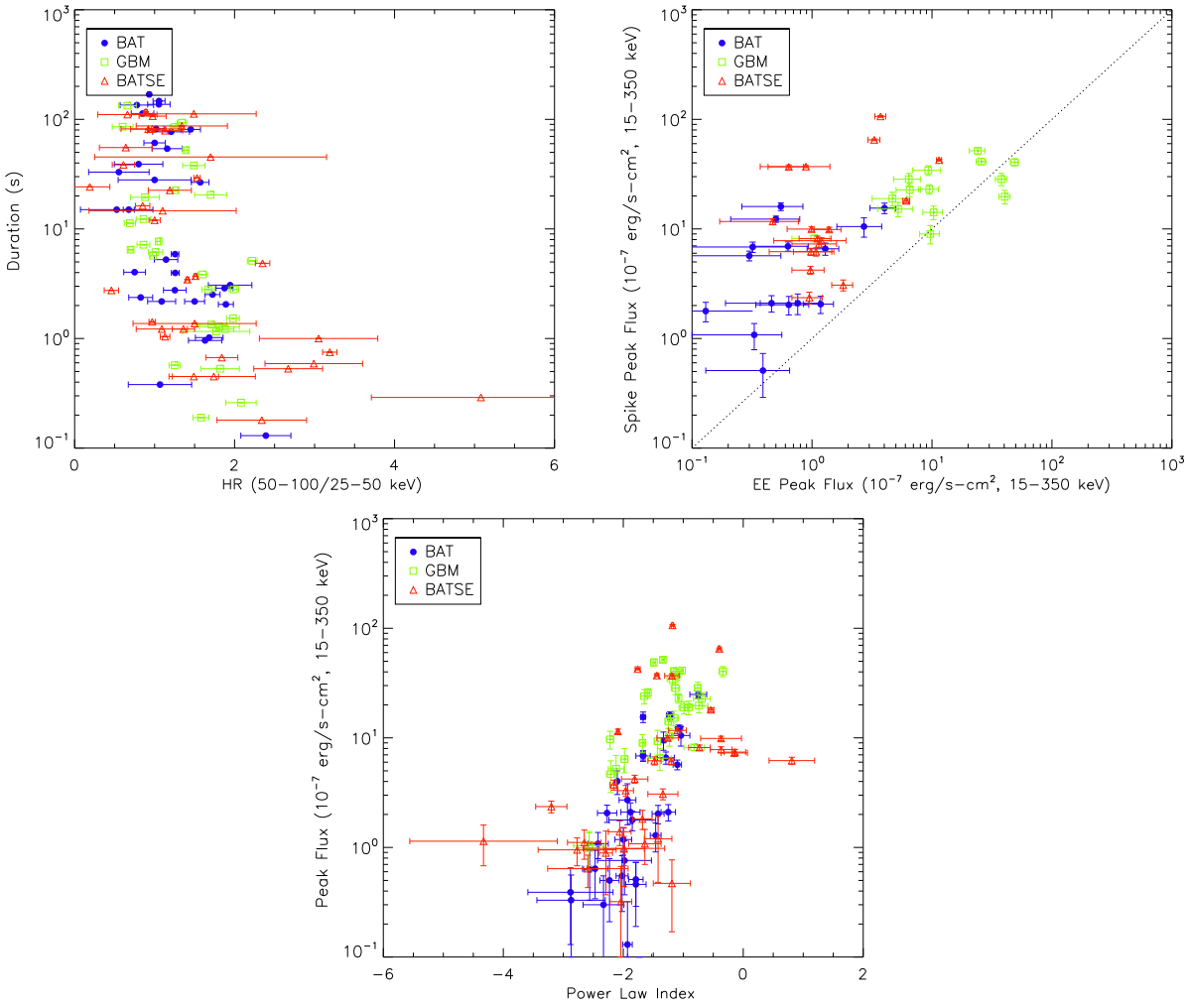

Figure 10. [*Top*] Duration ($T_{\rm spike}$ and $T_{\rm EE}$) vs. hardness ratio (*left panel*), spike peak flux vs. EE peak flux (*right panel*) for all GRBs with EE identified in BATSE, BAT, and GBM data. The dotted line shows the 1:1 line. [*Bottom*] Peak flux and spectral indices for both spike and EE components of all events. In all of the three parameter pairs, correlations with increased significance ($P \sim 10^{-14} - 10^{-6}$) were found when all datasets were combined.

5 DISCUSSION

We performed the most comprehensive investigations to date to search for EE that follow short GRBs observed with *Swift* BAT and *Fermi* GBM detectors. Based on the data availability and the filtering with the morphological criteria, the burst sample size subjected to our systematic search for the EE was 128 BAT and 287 GBM GRBs. These correspond to 19% and 28% of the total number of GRBs detected with BAT and GBM respectively, up until 2013 January 31. As a comparison, the fraction of GRBs classified as short-duration (< 2 s) event within the entire GRB data sample is 13% for BAT and 17% for GBM (Sakamoto et al. 2011; von Kienlin et al. 2014). Our search identified EE in 16 bursts seen with BAT, and 14 bursts with GBM. Of these three events are common in both EE samples, and two more events in the BAT samples were also observed with GBM but without the EE identified in the search. We see at least one event (GRB 100212A) of which the EE seen in the BAT coincided with what appeared as a X-ray flare in the XRT data.

None of these 30 candidates are considered "short" GRBs, by the conventional definition of $T_{90} < 2$ s. Even the duration of the spikes that we determined for our candidate events is mostly longer than 2 s, although the duration was calculated here using the lower energy ranges (<50 keV) than the standard energy range in which the duration is calculated for these instruments. Nonetheless, the negligible spectral lag of the spikes we found is consistent with short GRBs' properties. On the other hand, the duration of the EE components span a range of ∼10 s to ∼150 s, and the spectral lag we found for the EE is longer on average, being more consistent with long GRBs'.

The ratio of the energy emitted in the EE and in the spike (i.e., energy fluence ratio, $E_{\rm EE}/E_{\rm Spike}$) ranges from 0.21 to 33.5 (see Table 6), with a median value of 1.7 (1.99 for BAT sample and 1.67 for GBM sample). This means that for the majority of these events, more energy is emitted as EE than during the initial burst spike, significantly more in some cases. Interestingly, we found that $E_{\rm EE}$ is positively correlated with $E_{\rm Spike}$, which was revealed only when all datasets are considered together ($P = 7 \times 10^{-3}$).

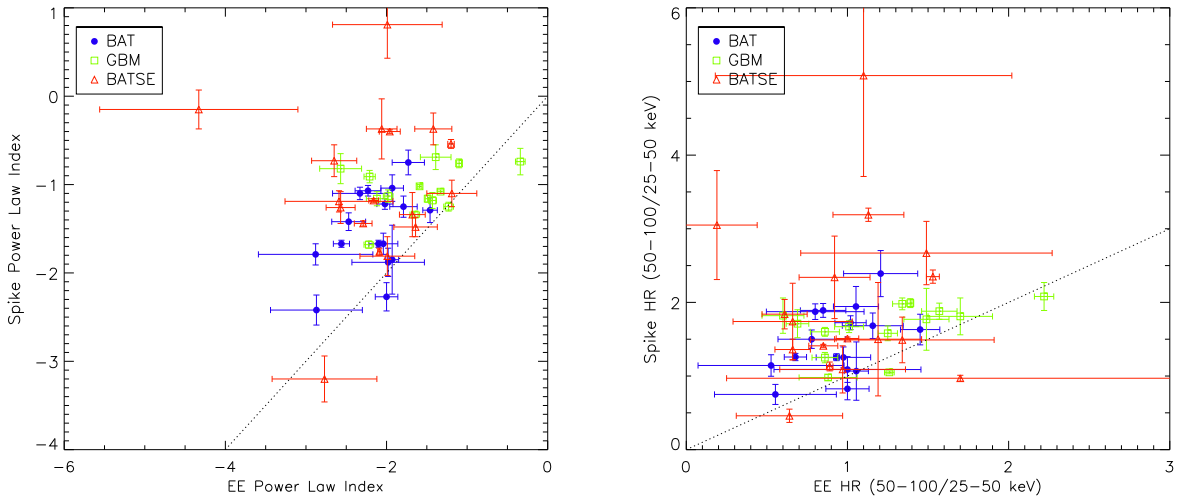

Figure 12. PWRL indices (*left*) and the hardness ratio (*right*) of the spikes vs. EE of the 30 candidate events. BAT and GBM events are shown with different symbols and colors. The 1:1 line is shown as dotted line. Although no correlations were found between these parameters, the plots indicate that the spikes tend to be spectrally harder than the EE. For comparison, the values for BATSE GRBs with EE from our previous work are also included.

We have also shown the cases where the burst is observed with both BAT and GBM (i.e., common event) but the EE was identified with only one of the detectors due to the difference in their sensitivities in a given energy range. Including also the cases where the EE was identified in both detectors' datasets, the joint spectral analysis yielded better constrained parameters.

5.1 Comparison with the BATSE events

Previously we identified 19 BATSE GRBs with EE using the same systematic search algorithm that we applied to the BAT and GBM data here (Bostancı, Kaneko & Göğüş 2013). The size of the sample subjected to the search was 296, i.e., 14% of all GRBs detected with BATSE in its entire mission. The number is actually smaller than the total number of short-duration BATSE GRBs (25% of all GRBs), due to the lack of orbital data used for the background estimation. This was not the case for the GBM data, and that increased the fraction of short-duration GBM GRBs included in the search sample.

Comparing the BATSE EE candidate events to the ones found here with BAT and GBM using the same search method, could reveal (or confirm the lack there of) any systematic differences between the instruments or biased preference of a detector towards detecting certain types of bursts. In Figure 10 we have shown the plots of three parameter pairs between which we found significant correlations. When each dataset (i.e., BAT, GBM, or BATSE) was individually studied, the correlations are only significant ($P > 10^{-4}$) in one or two of the datasets. Nevertheless, the correlations were found with much higher significance when all datasets were combined (Table 5). There in the peak flux plots, we see that most of the GBM events have higher peak flux in both spikes and EE than those of BAT and BATSE. In the top right-panel plot where the spike peak flux vs. EE peak flux is shown, it is also clear that the GBM events are with higher flux for both the spikes and the EE. This was also noticeable in terms of energy fluence of the spikes and the EE, with the GBM events offering the higher energy fluence on average than the BAT and BATSE events (see Figure 9).

The comparison between the general population of GRBs observed with GBM and with BATSE do not show much difference in their flux values as well as their spectral characteristics (Nava et al. 2011). Therefore, we suspect that the clear difference in the peak flux values found between the BATSE and GBM GRBs with EE is due to the significant difference in the detectors' effective area in the energy range where the EE components are most prominent. BATSE Large Area Detectors (as well as the BAT) had ∼10 times larger effective area than that of GBM NaI detectors below ∼100 keV (Tierney et al. 2013; Stamatikos 2009) where the EE components were usually detected. Thus, only the bursts associated with bright (i.e., higher peak flux) EE components were identified in our search using the GBM data. Then, the fact that the spike peak flux of these GBM events are also higher than the other (BAT and BATSE) events' is probably due to the strong positive correlation between the peak flux of the spikes and that of the EE components.

5.2 Two-Component Jet Model

In our previous study with the BATSE sample, we examined the two-component jet model of EE proposed by Barkov & Pozanenko (2011), by estimating the ratio of the opening angles of the two jet components ($\theta_{BZ}/\theta_{\nu\tilde{\nu}}$) for each of the candidate GRBs with EE. The angles were estimated based on the relation:

$$\frac{L_{BZ}}{L_{\nu\tilde{\nu}}}\left(\frac{\theta_{\nu\tilde{\nu}}}{\theta_{BZ}}\right)^2\frac{t_{BZ}}{t_{\nu\tilde{\nu}}}=\frac{E_{\rm EE}}{E_{\rm spike}}, \qquad (1)$$

where $E_{\rm EE}$ and $E_{\rm spike}$ are the observed energy fluence, and $t_{\nu\tilde{\nu}}$ and t_{BZ} are durations of the spike and the EE, respectively. Following Barkov & Pozanenko (2011), we used the luminosity estimates of $L_{BZ} \approx 10^{48}\,{\rm erg\,s^{-1}}$ and $L_{\nu\tilde{\nu}} \approx$

Table 6. Energy fluence ratio and the corresponding opening angle ratio estimates of the two jet components. GRB 111228 is excluded due to the insufficient statistics of its EE component to determine the energy fluence.

GRB name	$E_{\rm EE}/E_{\rm Spike}$ (15–350keV)	$\theta_{BZ}/\theta_{\nu\tilde{\nu}}$
BAT		
050724	1.69	0.28
051016B	0.64	0.21
060614	4.43	0.15
061006	1.16	0.40
061210	2.20	0.95
070506	0.22	0.21
070714B	0.26	0.41
080503	33.5	0.20
090531B	2.08	0.29
090927	0.87	0.22
100212A	1.99	0.32
100522A	0.36	0.19
110207A	6.69	0.15
110402A	3.01	0.19
111121A	1.09	0.28
121014A	6.28	0.21
GBM		
080807993	1.66	0.21
090131090	1.63	0.08
090820509	1.67	0.16
090831317	15.8	0.31
091120191	5.47	0.11
100517154	1.53	0.14
100522157	0.40	0.16
110207470	4.41	0.15
110402009	14.0	0.09
110824009	2.97	0.26
120402669	0.21	0.23
120605453	0.39	0.14
121029350	12.1	0.07

$3\times10^{50}\,{\rm erg\,s^{-1}}$ derived assuming typical physical parameters of the progenitor.

For comparison, we also estimate the jet opening angle ratios for our sample here, which we present in Table 6. We found that the angle ratio estimates with the BAT and GBM samples were smaller than those of the BATSE sample. This is likely due to the fact that the fluence ratio ($E_{\rm EE}/E_{\rm spike}$) of BAT and GBM samples are larger on average than those of the BATSE sample. Moreover, the BATSE GRBs with EE have shorter $T_{\rm spike}$ and longer $T_{\rm EE}$ on average than the BAT and GBM GRBs with EE, which makes $t_{BZ}/t_{\nu\tilde{\nu}}$ smaller for BAT+GBM samples and thus, $\theta_{BZ}/\theta_{\nu\tilde{\nu}}$ also smaller.

The angle ratio of the BAT and GBM GRBs estimated here span from 0.07 to 0.95, with a median value of 0.21. (they were 0.05 to 0.67, and 0.29 median for the BATSE sample). The neutorino-heated ($\nu\tilde{\nu}$) jet is expected to have an opening angle of $\sim$0.1, and the electromagnetic Blandford-Znajek (BZ) jet should have an opening angle that is inversely proportional to the Lorentz factor; $\theta_{BZ}\sim 1/\Gamma_{BZ}$. Then, the ratios we found here correspond to Γ_{BZ} of the order of 10−100, which is still in the range expected for the Lorenz factor of evolving BZ jet (Barkov & Pozanenko 2011).

ACKNOWLEDGMENTS

We thank the anonymous referee for his/her insightful and constructive suggestions, which significantly improved the paper. This project was supported by the Scientific and Technological Research Council of Turkey (TÜBİTAK grant 109T755).

REFERENCES

Band, D.L., et al. 1993, ApJ, 413, 281
Barkov, M.V. & Pozanenko, A., 2011, MNRAS, 417, 2161
Berger, E., 2014, ARAA, 52, 43
Bostancı, Z.F., Kaneko, Y., Göğüş, E., 2013, MNRAS, 428, 1623
Cobb, B.E., et al. 2010, ApJ, 718, L150
Eichler, D., Livio, M., Piran, T., Schramm, D. N., 1989, Nature, 340, 126
Fitzpatrick, G., Connaughton, V., McBreen, S., Tierney, D., 2011, arXiv: 1111.3779
Gehrels, N., et al., 2006, Nature, 444, 1044
Gruber, D. et al. 2014, ApJS, 211, 12
MacFadyen, A.I., Woosley, S.E., & Heger, A., 2001, ApJ, 550, 410
Nava, L., et al. 2011, MNRAS, 415, 3153
Norris, J. P., Marani, G. F., & Bonnell, J. T., 2000, ApJ, 534, 248
Norris, J. P. & Bonnell, J. T., 2006, ApJ, 643, 266
Norris, J.P., Gehrels, N., & Scargle, J.D., 2010, ApJ, 717, 411
Norris, J.P., Gehrels, N., & Scargle, J.D., 2011, ApJ, 735, 23
Paciesas, W.S., et al. 2012 ApJS 199 18
Sakamoto, T., et al. 2011, ApJS, 195, 2
Scargle, J.D., et al., 2013, ApJ, 764, 167
Stamatikos, M., 2009, arXiv:0907.3190
Tierney, D., et al., 2013, A&A, 550, A102
Thompson, T.A., Chang, P. & Quataert, E. 2004, ApJ, 611, 380
Ukwatta, T.N., et al. 2010, ApJ, 711, 1073
von Kienlin, A., et al. 2014, ApJS, 211, 13
Woosley, S.E., 1993, ApJ, 405, 273.
Woosley, S.E. & Bloom, J.S. 2006, ARAA, 44, 507